ARTICLE

Optimization of Failure-Tolerant Workspaces for Redundant Manipulators

Rodrigo S. Jamisola, Jr.

Electronics and Communications Engineering Dept. De La Salle University – Manila 201 Taft Ave., 1004 Manila

For a redundant manipulator a region in its workspace that is guaranteed failure tolerant, called the failure-tolerant workspace, promises completion of critical tasks placed within it. By judiciously choosing a set of artificial joint limits which constrain the acceptable robot configurations prior to a failure, a failure-tolerant workspace can possibly exist even for manipulators with a single degree of redundancy. This work identifies the candidate boundaries of failure-tolerant workspaces, and presents justification on their validity and completeness. Based on the identified boundaries, optimization results for a 3-degree-of-freedom (dof) planar manipulator, as well as for a 4-dof planar manipulator, are presented. It assumed that the manipulator has the ability to lock a joint that has failed, and that the manipulator's workspace degree of freedom remains the same before and after a joint failure.

KEYWORDS
robotics, robot motion planning, kinematics failure tolerance, reachable workspace, optimization

I. INTRODUCTION

An extra joint in kinematically redundant manipulators creates greater dexterity in task execution. For the end-effector location of a kinematically redundant manipulator, an infinite number of postures (called configurations) correspond to the same workspace location. With the extra joint, the redundant manipulator can perform the required workspace task and, at the same time, vary its posture to perform obstacle avoidance, manipulability optimization, failure tolerance, and other desired posture optimization criteria.

In this work, the posture optimization criterion would be that of tolerance to joint failure, such that the manipulator would be able to perform the required workspace task before and after the occurrence of a joint failure. The manipulator joints are allowed to be locked in failure such that the workspace degree of freedom remains constant.

Tolerance to joint failure has gained popularity among robot researches because, when addressed properly, the robot manipulator can be guaranteed to complete critical tasks despite one or more of its joints failing. This is especially applicable when the robot is tasked to perform work in remote or hazardous environments where direct human intervention, in the case of joint failures, is not possible. For example, robots working in nuclear waste disposal or robots that perform deep underwater explorations, or robots that are sent to space. In these cases, robot repair during joint failures could mean additional cost due to the delay, or could possible pose danger to human life.

When a failure-tolerant workspace for a given robot is already identified, the robot user will only have to specify locations of critical tasks to be within this region in order to guarantee completion despite one or more of the robot's joints failing. Further, identifying the maximum possible region of such a workspace would mean more tasks that can be possibly specified at a given time for the manipulator.

Email Address: rodrigo.jamisola@dlsu.edu.ph
Submitted: August 29.2009
Revised: March 24, 2010
Accepted: March 24, 2010
Published: April 16, 2010
Editor-in-charge: Eduardo A. Padlan

From the pioneering work on kinematic failure tolerance for redundant manipulators (Maciejewksi 1990), many related studies have been performed. These include design enhancement for failure tolerance including kinematic redundancy and dual actuation (Monteverde and Tosunoglu 1997), presentation of an analysis tool to determine the fault-tolerant workspace when no joint limits are considered (Paredis and Khosla 1994), failure tolerance in the domain of mechanical systems (Sreevijayan et al. 1994), failure tolerance by considering both kinematics and dynamics of the manipulator (Li and Gruver 1998), examination of the reduced manipulability of a manipulator after one or more joint failure (Roberts and Maciejewski 1996), real-time implementation (Groom et al. 1999), and when obstacles in the environment are considered (Paredis and Khosla 1996).

Among the more recent studies in kinematic failure tolerance include failure tolerance for cooperative manipulators rigidly connected to a solid object (Tinos et al. 2002), fault detection and tolerance for static walking of rigid robots, where each leg has three revolute joints (Yang 2002), fault tolerance for parallel manipulators using task space and kinematic redundancy (Yi et al. 2006), characterization of optimally fault-tolerant manipulators based on relative manipulability index (Roberts et al. 2007), designing the nominal manipulator Jacobian for optimal fault tolerance to one or more joint failures, especially for parallel mechanisms (Roberts et al. 2008), quantification of optimal faut-tolerant manipulability for Stewart platforms (Ukidve et al. 2008), and using neural network for failure-tolerant control of redundant robots (Srinivasa and Grossberg 2007).

A new approach to obstacle avoidance with failure tolerance is shown in Jamisola et al. (2003) and Jamisola et al. (2006). The existence of an obstacle-free surface in the configuration space (C-space) with no local minimum guarantees task completion despite joint failures and obstacles in the workspace. Start and goal locations were specified and the position of the obstacles was known. A related problem to the mentioned work is to identify the workspace region that is known to be tolerant to failure, without consideration for obstacles. A previous work (Paredis and Khosla 1996) stated that one needs at least two degrees of redundancy for a failure-tolerant workspace to exist on a given redundant manipulator. This limitation was overcome by imposing artificial joint limits prior to a failure (Lewis and Maciejewski 1997). Because reachability of workspace locations after a failure is dependent on the manipulator configuration at the instance of failure, constraining the allowable joint values prior to a failure will ensure certain workspace locations to remain reachable after a joint failure.

A more recent work showed that the boundaries of the failure-tolerant workspace are identifiable (Roberts et al. 2007). This removed significant computational burden because, instead of computing for the entire failure-tolerant region, only its boundaries are identified. However, for much higher degrees of redundancy this may not be necessarily true.

This work will try to build on the results of Roberts et al. (2007) and will present justifications on the validity and completeness in identifying the candidate boundaries of the failure-tolerant workspace. In addition, optimal results and analysis for a 3-dof planar manipulator with constant and variable link lengths, as well as for a planar 4-dof manipulator with constant link lengths, will be presented. Planar manipulators are chosen as implementation platforms for simplicity and clearer presentation of results. The 3-dof planar manipulator (both constant and variable link lengths) is used to illustrate the case where only a single joint failure is allowed, while the 4-dof planar manipulator (with equal link lengths) is shown for the case where one or two joints can fail at any given time. Higher degrees of freedom workspaces will be considered in future implementations.

II. AN OVERVIEW OF THE PROPOSED APPROACH

Before proceeding with the gradient method of identifying the optimal failure-tolerant workspace, a global brute-force computation of the 3-dof robot with equal link lengths was performed. The value of the artificial joint limits was varied and the corresponding failure-tolerant workspaces are computed. The results shown in Fig. 1, which approximately agrees with the optimal results found in Lewis and Maciejewski (1997), gave a global perspective on the extent of the failure-tolerant workspace region as the artificial joint limits were varied. For redundant manipulators, a workspace location $\mathbf{x} \in \mathsf{R}^m$ and a manipulator configuration $\mathbf{q} \in \mathsf{R}^n$ such that $n > m$. The Jacobian matrix relates the incremental change in the manipulator configuration, $\delta\mathbf{q}$, to that of the incremental change in the manipulator end-effector location, $\delta\mathbf{x}$,

$$\delta\mathbf{x} = \mathbf{J}\ \delta\mathbf{q} \quad (1)$$

where $\mathbf{J} \in \mathsf{R}^{m\times n}$. A given manipulator's reachable workspace, without consideration to joint failures, will be called a normal workspace and labeled W. When joint failures are considered, the resulting reachable workspace after a failure is dependent on the manipulator configuration at the instance of failure. Thus the resulting failure-tolerant workspace is dependent on the allowable range of joint values imposed on the manipulator prior to a failure. For a given manipulator, the problem becomes that of searching for a set of artificial joint limits that will maximize the failure-tolerant workspace. In the event of a joint failure, the artificial joint limits are released and the physical limits become the new joint limits. The failure-tolerant workspace is labeled W_S (S for "safe"). A reachable workspace location is tolerant to a joint failure if it remains reachable after a failure. This location is labeled as $\mathbf{x}_S$ such that $\mathbf{x}_S \in W_S$. Because the manipulator configuration at the instance of failure is not known, one has to consider all the possible W's for every possible joint failure to be able to identify W_S. The intersection of all the possible workspaces corresponding to every possible joint failure(s) is labeled W_F (F for "failed"). This workspace can also be interpreted as the workspace that is guaranteed reachable after

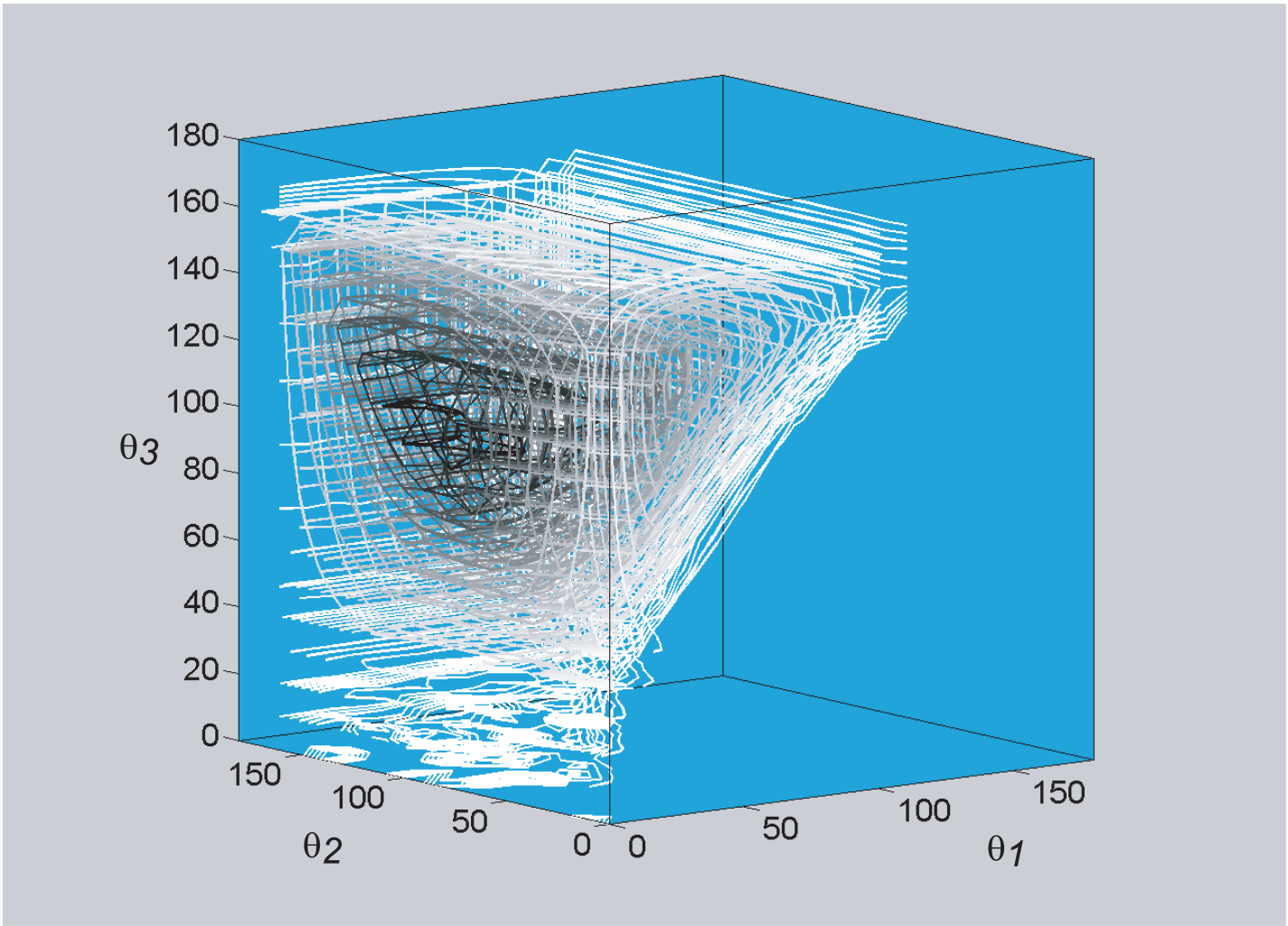

Figure 1. A global plot of the failure-tolerant workspace for a 3-dof planar manipulator with equal link lengths. The plot has a resolution of 10 degrees such that the black contours are approximately 4000 sq. units, the gray contours are approximately 2000 sq. units, and the white contours are approximately 1 sq. unit. It is shown that the maximum area lies around the range of θ_1 = [0,50], θ_2 = [50,150], and θ_3 = [80,120] degrees.

any joint failure. The reachable workspace prior to a joint failure is labeled W_O (O for "original"). The resulting W_S is the intersection of W_F and W_O,

$$W_S = W_O \cap W_F \,. \quad (2)$$

Techniques will be discussed on how to identify the boundaries of W_S to ease the burden of computation.

III. CANDIDATE BOUNDARIES OF THE FAILURE-TOLERANT WORKSPACE

For a normal workspace W, a reachable workspace location **x** lies at the boundary if there exists a small incremental displacement δ**x** such that **x** + δ**x** is not reachable. It is

characterized by either a manipulator singularity or a joint limit singularity, also called semi-singularity (Luck 1995). This is formally stated below.

Definition 1. *The boundaries of a normal workspace are characterized by either manipulator singularities or joint limit singularities.*

When a joint failure occurs, the resulting failed manipulator will have a corresponding new reachable workspace W' whose boundaries now correspond to the singularities of the resulting failed manipulator and singularities of the new joint limits. From Eqn. 2 and assuming W_S exists, the boundaries of W_S are characterized by the singularities of the original manipulator, the singularities of the failed manipulator, and the joint limit singularities. At this point, we have sufficiently described the candidate boundaries of W_S. Let us formally present this statement below.

The boundaries of a failure-tolerant workspace can be characterized by three types of manipulator singularities:

- Singularity of the original manipulator
- Singularity of the failed manipulator
- Joint limit singularity

Justification for their validity will be presented. Because the workspaces consisting W_F are infinitely many, further discussion will be given on how to identify the boundaries of W_F by considering only a number of workspaces that make up its boundaries. The true boundaries of W_S can be determined by checking the tolerance to failure of every candidate boundary.

A. Singularity of the Original Manipulator

Given a configuration **q** such that $\det(\mathbf{J}\mathbf{J}^T)=0$. At $\mathbf{x} = \mathbf{f}(\mathbf{q})$ the manipulator loses at least one degree of freedom such that there exists an $\mathbf{x}+\delta\mathbf{x}$ that is not reachable. The location **x** is said to correspond to an escapable singularity if there exists a different configuration **q'** such that $\mathbf{x} = \mathbf{f}(\mathbf{q'})$ and $\mathbf{x}+\delta\mathbf{x}$ becomes reachable for all $\delta\mathbf{x}$'s. In this case, **x** does not lie on a true boundary of W .

On the other hand, a different location **x** is said to correspond to an inescapable singularity if $\mathbf{x}=\mathbf{f}(\mathbf{q})$ and $\det(\mathbf{J}\mathbf{J}^T)=0$ for all **q**'s corresponding to **x**. In this case, **x** lies at a workspace boundary. In equation form,

$$\mathbf{x} \in \partial W \text{ if } \mathbf{x} = \mathbf{f}(\mathbf{q}) \text{ and } \det(\mathbf{J}\mathbf{J}^T)=0 \quad \forall \mathbf{q} = \mathbf{f}^{-1}(\mathbf{x}) \quad (3)$$

where ∂W is the boundary of the workspace W. We are now ready to characterize the singularity of the original manipulator as a candidate boundary of W_S.

Lemma 1: Singularity of original manipulator characterizes a candidate boundary of the failure-tolerant workspace.

Proof: From Def. 1, the singularity of the original manipulator characterizes the boundaries of W_O, such that a workspace location **x** corresponding to an inescapable singularity lies exactly at the boundary of W_O from Eqn. 3. By Eqn. 2, a boundary of W_O may lie at the boundary of W_S which makes the singularity of the original manipulator a candidate boundary of W_S.

In an event of a failure, an escapable singularity of the original manipulator may become an inescapable singularity of the resulting failed manipulator. This will correspond to the second candidate boundary of W_S.

B. Singularity of the Failed Manipulator

Let $\mathbf{J}_F$ be the Jacobian of the resulting manipulator after a failure where the corresponding column(s) of the failed joint(s) is truncated, such that $\mathbf{J}_F \in \mathbb{R}^{m\times p}$ and $p=n-1,\ldots,m$. To search for the singularity of the every possible failed manipulator is to search for every possible $\mathbf{J}_F$ and its corresponding $\det(\mathbf{J}_F\mathbf{J}_F^T) = 0$.

Lemma 2: Singularity of the failed manipulator characterizes a candidate boundary of the failure-tolerant workspace.

Proof: Let us consider that the failed manipulator is a different manipulator that is independent from the original one. By Def. 1, the new workspace boundaries can be characterized by the singularities of its corresponding new manipulator, such that the inescapable singularities exactly lie at its boundaries. Because W_F results from the intersection of all these possible new workspaces, from Eqn. 2 the boundaries of each new workspace are possible boundaries of W_F as well as of W_S.

Not all new workspaces resulting from a failure will define the boundaries of W_F. It is imperative to be able to characterize the boundaries of W_F to lessen the computational burden.

C. Joint Limit Singularity

Joint limit singularity is further subdivided into two types: tangent and edge singularities. A tangent singularity is equivalent to the singularity of the failed manipulator when the joint failed at the limit. An edge singularity corresponds to a configuration at the edge (or corner) of the C-space.

Lemma 3: Joint limit singularity characterizes a candidate boundary of the failure-tolerant workspace.

Proof: By Definition 1, joint limit singularities characterize the boundaries of W_O. For every possible joint failure, a new set of joint limits will characterize each resulting manipulator's workspace, and are candidate boundaries of W_F as well as of W_S.

As in the failed manipulator singularity, the joint limit singularity also considers every possible failed manipulator's workspace. This section sufficiently identifies all the candidate boundaries of W_S.

IV. CHARACTERIZING THE CANDIDATE BOUNDARIES OF W_F

To present justification for the candidate boundaries of W_F, we first introduce the concept of *self-motion manifolds*. The self-motion manifolds of workspace location $\mathbf{x} = \mathbf{f}(\mathbf{q})$ are disjoint connected subsets of the pre-image $\mathbf{f}^{-1}(\mathbf{x})$. Given a manipulator with *r*-degree of redundancy,

$$\mathbf{f}^{-1}(\mathbf{x}) = \bigcup_{i=1}^{N} M_i \quad (4)$$

where M_i is the *r*-th dimensional self-motion manifold and *N* is the number of self-motion manifolds, such that when $i \neq j$, $M_i \cap M_j = \varnothing$ (Burdick 89).

From Eqn. 2 and given a failure-tolerant workspace location **x** we can state that

$$\mathbf{x} \in W_S \Leftrightarrow \mathbf{x} \in W_O \text{ and } \mathbf{x} \in W_F \text{ . (5)}$$

The first term can be satisfied if there exists at least one configuration **q** such that **x** = **f(q)** is reachable before a joint failure. The second term is trickier by the fact that for a given workspace location **x**, there must exist a connected portion of the self-motion manifold, within the joint limits, that can maintain reachability of **x** after a joint failure. This will guarantee reachability of **x** for any joint failures within the set limits.

Definition 2. *A workspace location is guaranteed reachable after a joint failure if there exists a connected portion of the self-motion manifold that spans the entire range of values within the joint limits.*

We are now ready to identify the candidate boundaries of W_F. This is stated as a theorem below.

Theorem 1: The changes in the topology of the C-space characterize the candidate boundaries of W_F.

Proof: The satisfaction of the failure-tolerance test, i.e., reachability of **x** for any joint failure, is dependent on the connectedness of the corresponding self-motion manifold within the set limits. A topological change in the C-space results in a characteristic change of the self-motion manifolds and their connectedness. As a manipulator configuration passes through a topological change in the C-space, the satisfaction of the failure-tolerance test can vary. Such possible variation in the satisfaction of the failure-tolerance test characterizes the candidate boundaries of W_F.

The changes in the C-space topology can be internal or at a C-space boundary. An internal C-space topological change occurs at the original manipulator's singularity, while the topological change at the C-space boundary occurs at a joint limit singularity.

The self-motion manifold corresponding to an escapable singularity of the original manipulator may span an entire range of a set of joint values in the configuration space.

When this set of joint values corresponds to the possible joint failures, failure tolerance is guaranteed. Its adjacent self-motion manifolds may not be connected within the limit.

The self-motion manifold that is tangent at a joint limit has the possibility of satisfying the failure-tolerance test for the corresponding joint. Close to it, there exits another self-motion manifold that fell short of touching the joint limit and therefore cannot satisfy the connectedness within the limit.

At the edge of the C-space, a self-motion manifold intersects more than one joint limit. This self-motion manifold may satisfy the failure-tolerance test for the corresponding joint limit. At its vicinity, another self-motion manifold that intersects only one joint limit cannot satisfy the failure-tolerance test of the other joint limit.

Now that the candidate boundaries of W_F are identified, the candidate boundaries of W_S are modified as follows:

- Singularity of the original manipulator
- Tangent singularity
- Edge singularity

The next subsection will be a step-by-step approach of finding the candidate boundaries of W_S.

V. ALGORITHM OF THE PROPOSED APPROACH

Consider that a failure-tolerant workspace exists for a given manipulator and a set of artificial joint limits. The boundaries of W_S are identified through the following steps:

1) Search for the singularities of the original manipulator, $\det(\mathbf{J}\mathbf{J}^T) = 0$, and compute their corresponding workspace locations.
2) Search for the tangent singularities such that $\det(\mathbf{J}_F\mathbf{J}_F^T) = 0$ for $p = n - 1,\ldots,m$, and compute for their corresponding workspace locations.
3) Search for the edge singularities and compute for their corresponding workspace locations.
4) Determine the intersections between the candidate boundaries.
5) Test each segment of the candidate boundaries for tolerance to joint failures.

VI. OPTIMAL FAILURE-TOLERANT WORKSPACES

The optimal results shown in this work used planar workspaces. The joint limits are symmetric and so are the resulting W_S's thus the area computation is performed on one side of W_S and is multiplied by two. Symmetry of the joints limits are commonly used by industrial robots. The area of the failure-tolerant workspace was computed by taking the integral for each true boundary over a free joint, that is,

$$A_{WS} = 2 \sum_{i=1}^{n_B} \int_{q_{ia}}^{q_{ib}} \mathbf{B}\, dq_i \text{ (6)}$$

where A_{WS} is the area of W_S, **B** is a segment of the true boundary, q_{ia} and q_{ib} are the limits of the free joint q_i, and n_B is the number of segments of the true boundary. Optimization computation was performed using the gradient ascent method such that at every computational cycle t,

$$\mathbf{v}^{(t+1)} = \mathbf{v}^{(t)} + \left[\gamma \frac{\partial A_{WS}}{\partial \mathbf{v}} \right]^{(t)} \text{ (7)}$$

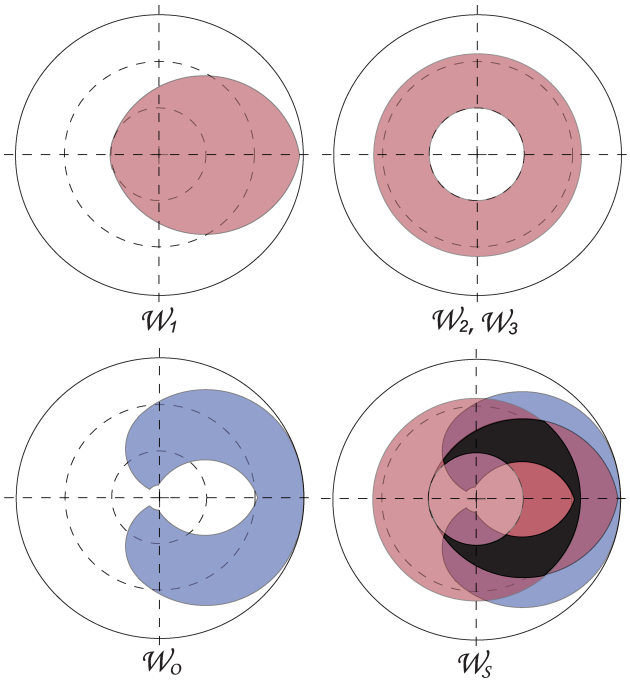

Figure 2. The optimal W_S for a 3-dof robot with equal link lengths is shown. The workspaces W_1, W_2, and W_3 are the W_F 's for the corresponding joint failure. The symmetric artificial joint limits are $[(+/-)18, (+/-)111, (+/-)111]^T$ degrees, and W_S has an area of 3.56 sq. units where each link has 1 unit length.

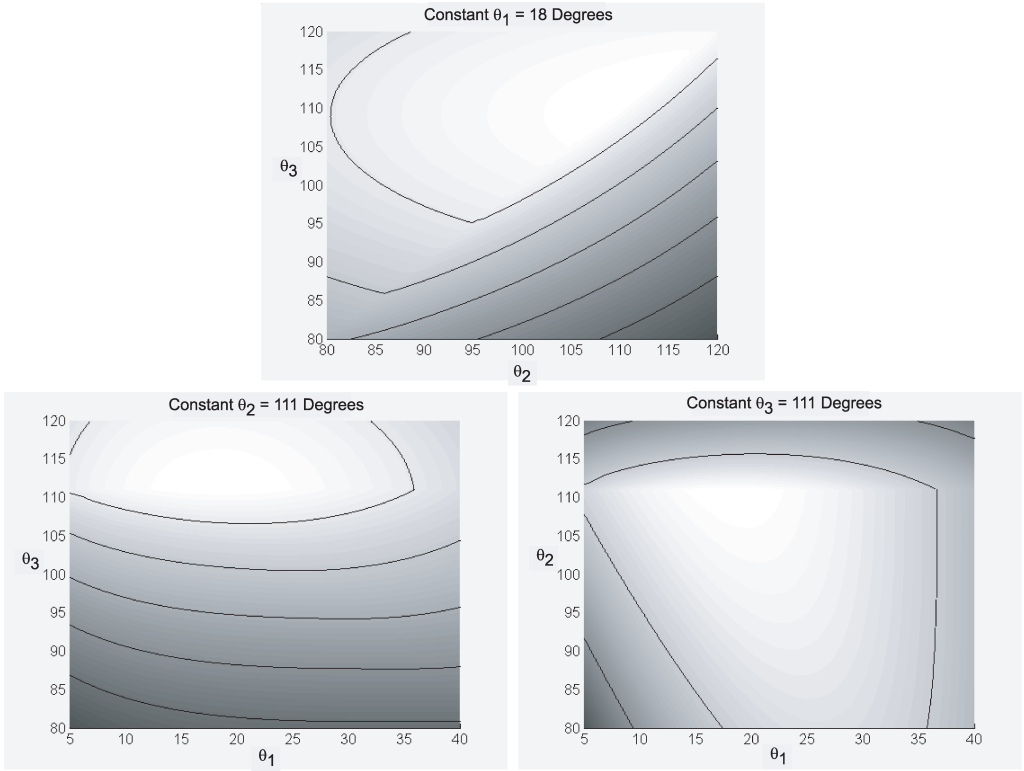

Figure 3. The figure shows the plots of A_{WS} at the slices of the optimal artificial joint limits of $[(+/-)18, (+/-)111, (+/-)111]^T$ degrees for the 3-DOF planar robot with equal link lengths. The contour lines are at 0.313 sq. units apart. The white portion shows the vicinity of the optimal A_{WS}.

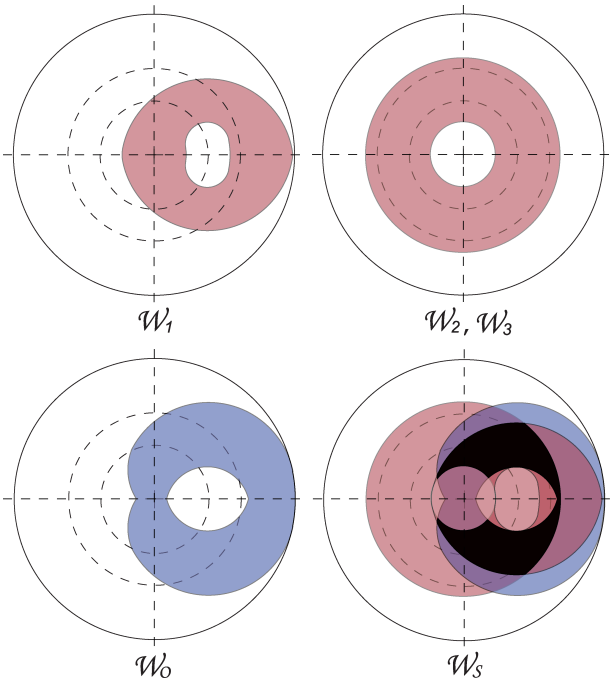

Figure 4. The figure shows the optimal W_S of a 3-dof robot that is kinematically designed to maximize A_{WS} = 3.71 sq. units. The optimal W_S is shown as the black region. The link lengths are $[1.2,0.6,1.2]^T$ units with symmetric artificialjoint limits of [(+/-)11, (+/-)128, (+/-)128] degrees

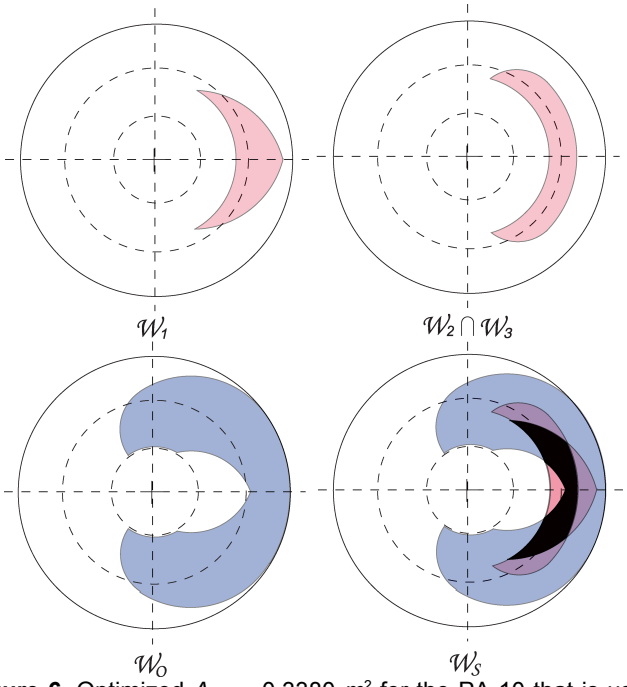

Figure 6. Optimized A_{WS} = 0.3380 m^2 for the PA-10 that is used as a 3-dof planar robot is shown. The link lengths are $[0.45,0.5,0.45]^T$ m, the artificial joint limits are [(+/-)32, (+/-)92, (+/-)92]^T degrees, and the physical limits are [(+/-)90, (+/-)135, (+/-)160]^T degrees.

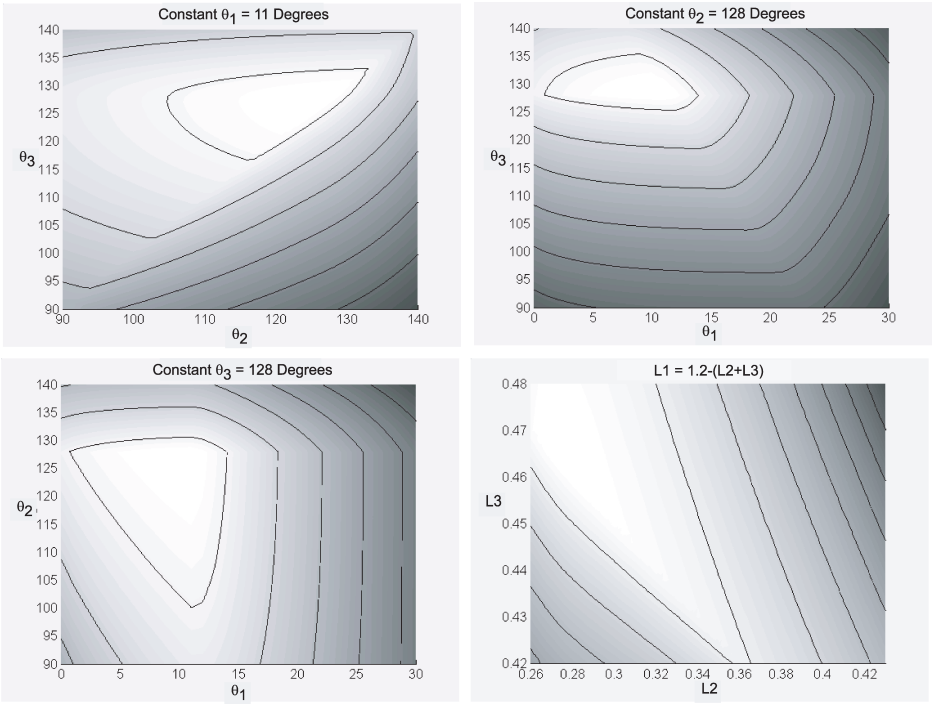

Figure 5. The figure shows slices at the optimal A_{WS} in Fig. 4. The contour lines are at 0.313 sq. units apart. The white portion shows the vicinity of the optimal A_{WS} . Three subfigures show the slices where one of the optimal artificial joint limits and the optimal link lengths are held constant. The fourth subfigure showed $L1 = 1.2-(L2+L3)$, and all optimal artificial limits are constant.

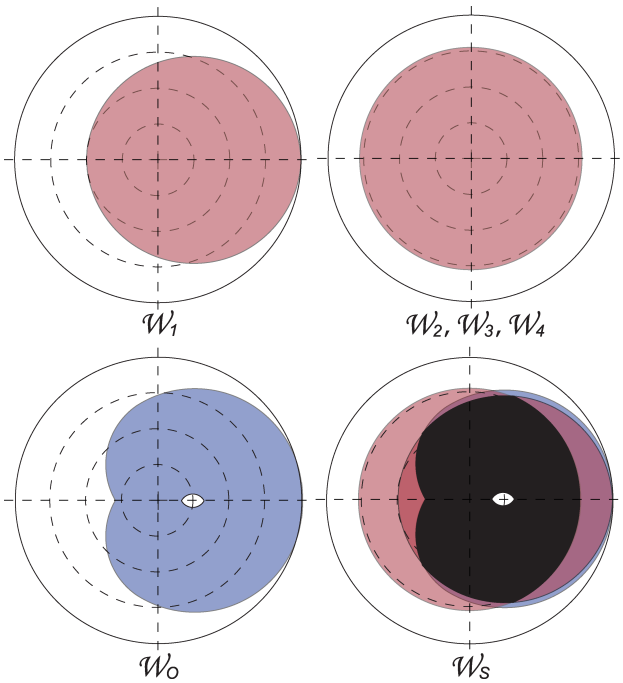

Figure 7. The figure shows the corresponding workspaces for a 4-dof planar robot with equal link lengths [0.3,0.3,0.3,0.3]T units and the optimal artificial limits [(+/-)7, (+/-)110, (+/-)110, (+/-)110]^T degrees such that its workspace is identical to that of the 3-dof planar robot.

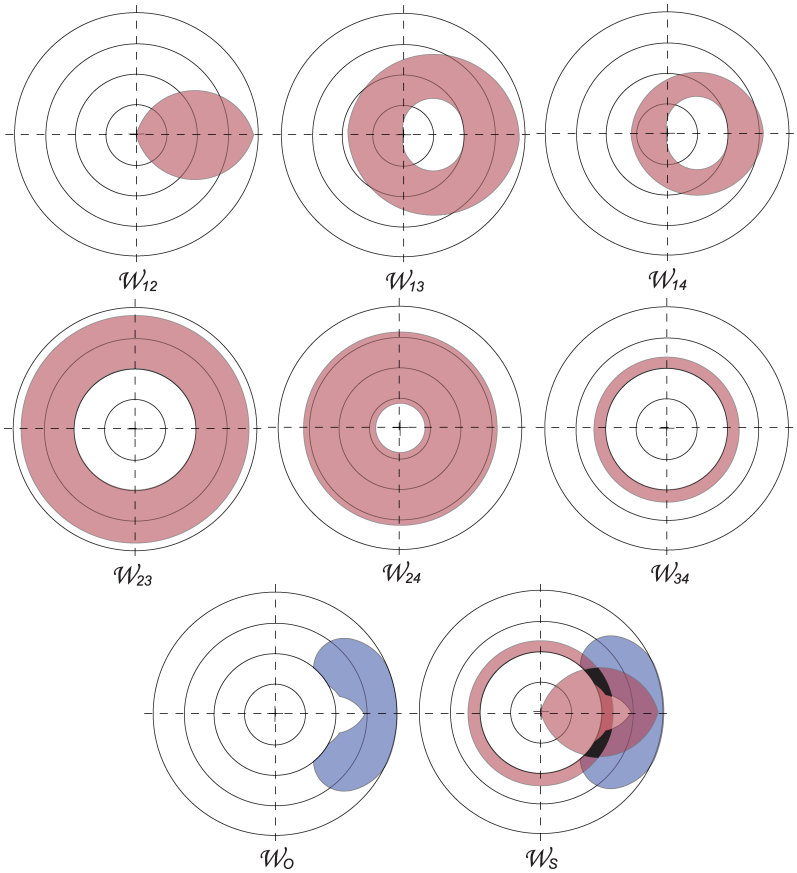

Figure 8. An optimal case for a 4-dof planar with two joints failing is shown in the figure that has an area of A_{WS} = 0.0581 sq. units. The link lengths are equal at [0.3,0.3,0.3,0.3]^T units and the artificial joint limits are [(+/-)11, (+/-)11, (+/-)48, (+/-)107]^T .

where **v** can be a function of both artificial joint limits and link lengths when manipulator design is considered, and γ is the step size. Because the computation is local in nature, random starting values for the variable **v** were used, and random steps around the vicinity of a local maximum were taken until the maximum allowable computational cycle is reached. The vicinity of the optimal value for the 3-dof equal link length case has been previously known from the brute-force computation, so the starting configuration for this case was easily chosen.

Optimization results for 3-dof planar robot with equal link lengths, and of a 3-dof planar robot with variable link lengths will be presented. To support the validity of these results, the information regarding the C-space slices at the optimal failure-tolerant workspace value is shown. In addition, optimal results of the PA-10 robot that is used as a 3-dof planar robot, of a 4-dof planar robot with single joint failure, and of a 4-dof planar robot with 2-joint failure are presented.

Optimal results of a 3-dof planar robot with equal link lengths are shown in Fig. 2. The workspaces W_i's are the W_F's for the corresponding joint i. Slices at the optimal value of A_{WS} corresponding to a symmetric artificial joint limits of $[(+/-)18, (+/-)111, (+/-)11]^T$ are shown in Fig. 3. The white portion is the vicinity of the optimal value. At each slice, an artificial joint limit value is held constant while the other two artificial joint limits are linearly varied. The contour lines are at 0.313 sq. units apart. This optimal value is a 13% increase to that found in Lewis and Maciejewski (1997).

The ridge for each subfigure in Fig. 3 corresponds to the switching of the candidate boundary (due to tangent singularity) between W_2 and W_3, depending on which one is a true boundary. The artificial joint limits for joints 2 and 3 have to be equal to maximize the region of intersection between W_2 and W_3. Its outer boundary is the most influential boundary of W_S such that a change in the joint 2 or 3 value can significantly decrease the area of W_S, as shown in Fig. 3.

The second case considers a 3-dof planar robot such that its links are allowed to vary in lengths. The resulting W_O is identical to the equal link length case. The optimal result has a link lengths of $[1.2,0.6,1.2]T$, and the artificial joint limits are $[(+/-)11, (+/-)128, (+/-)128]^T$ degrees. Due to the links not being equal, W_1 has an inner boundary as shown in Fig. 4. Intuitively, one may think that the optimal value of A_{WS} compared to the equal link case is lesser because of this. However in the resulting optimal W_S, the hole did not have any contribution when all its corresponding boundaries were intersected. In addition, the location of the inner boundary of W_2 and W_3 is closer to the origin compared to the equal link length case. The resulting A_{WS} has a 4.2% increase from the equal link length case.

Slices at the optimal A_{WS} for the 3-dof with variable link lengths are shown in Fig. 5. For the first three subfigures, two joint limits values are varied and the other joint limit and the link lengths are held constant at the optimal value. The fourth subfigure held the optimal artificial joint limits constant while the $L2$ and $L3$ link lengths are varied, such that $L1 = 1.2 - (L2 + L3)$. Ridges on the topology have similar characteristics as those of the equal link length case, for the subfigures where the link lengths are held constant and the joint values are changing. An additional ridge that is less sharp is due to the hole in the workspace created by the inner boundary of W_1. The ridge in fourth subfigure is caused by the switching of the boundaries of W_2 and W_3, whichever becomes the true boundary.

Optimization of A_{WS} for the PA-10 that is used as a 3-dof planar robot is shown in Fig. 6. Links 2, 4, and 6 with link lengths $[0.45,0.5,0.45]$ m and physical limits $[(+/-)90, (+/-)135, (+/-)160]^T$ degrees were used. The rest of the links were locked. At the optimal $A_{WS}=0.3380$ m^2 the artificial joint limits are $[32, 92, 92]^T$ degrees. This example shows the case when physical limits were present. It upholds the fact that present industrial robots with a single degree of redundancy have the ability to become failure tolerant by judiciously constraining the joint values prior to a failure.

In considering the 4-dof planar robot, the link lengths were chosen to be equal to each other at $[0.3,0.3,0.3,0.3]^T$ units such that its W_O is identical to that of the 3-dof equal link length case. For a single locked-joint failure, the problem becomes that of a 3-dof planar robot where one of its link lengths is derived from the configuration of the locked joint. The optimal results are shown in Fig. 7. The optimal A_{WS} = 1.9115 sq. units and the corresponding set of artificial joint limits are $[(+/-)7, (+/-)110, (+/-)110,(+/-)110]^T$ degrees. The shown optimal A_{WS} is 3.2 times that for the kinematically designed.

When two joints are allowed to fail in the 4-dof planar robot, the optimal W_S area is reduced significantly as shown in Fig. 8. The workspaces W_{ij}'s are the W_F's for the corresponding joints i and j. Not all W_F's from two joints failing define the boundaries of W_S. It is shown that the boundaries are defined by W_O, W_{12}, and W_{34}.

VII. SUMMARY AND CONCLUSION

This work has characterized the candidate boundaries of failure-tolerant workspaces, and has presented justifications on their validity and completeness. Optimal results for planar manipulators with single as well as double joint failures were presented. This work further supported the claim that failure-tolerant workspaces exists, even for present industrial robots with a single degree of redundancy. Future research work is geared towards optimizing failure-tolerant workspaces for full-spatial redundant manipulators.

VIII. ACKNOWLEDGEMENTS

The author gratefully acknowledges the contributions of Prof. Anthony A. Maciejewski and Prof. Rodney G. Roberts.

REFERENCES

Burdick JW. On the inverse kinematics of redundant manipulators: Characterization of the self-motion manifolds. In IEEE Int Conf Robot Automat, pages 264–270, Scotsdale, AZ, May 14-19, 1989.

Groom KN, Maciejewski AA, Balakrishnan V. Real-time failure-tolerant control of kinematically redundant manipulators. IEEE Trans Robot Automat 1999; 15:1109–1116.

Jamisola RS Jr, Maciejewski AA, Roberts RG. A path planning strategy for kinematically redundant manipulators anticipating joint failures in the presence of obstacles. In IEEE/RSJ Int Conf Intell Robots Syst, pages 142–148, Las Vegas, NV, Oct 27-31, 2003.

Jamisola RS Jr, Maciejewski AA, Roberts RG. Failure-tolerant path planning for kinematically redundant manipulators anticipating locked-joint failures. IEEE Trans Robot 2006; 22:603–612.

Li L, Gruver WA. Fault-tolerant control of redundant robots by dual-optimization. In IEEE/RSJ Int Conf Intell Robots Syst, pages 336–341, Victoria, Canada, Oct 13-17, 1998.

Lewis CL, Maciejewski AA. Fault tolerant operation of kinematically redundant manipulators for locked joint failures. IEEE Trans Robot Automat 1997; 13:622–629.

Luck CL. Robot Cartography: A Topology-Based Representation for the Global Kinematic Control of Redundant Manipulators under Constraints. PhD thesis, Univ. of South. California, 1995.

Maciejewksi AA. Fault tolerant properties of kinematically redundant manipulators. In IEEE Int Conf Robot Automat, pages 638–642, Cincinnati, OH, May 13-18, 1990.

Monteverde V, Tosunoglu S. Effect of kinematic structure and dual actuation on fault tolerance of robot manipulators. In IEEE Int Conf Robot Automat, pages 2902–2907, Albuquerque, NM, April 20-25, 1997.

Paredis CJJ, Khosla PK. Mapping task into fault tolerant manipulators. In IEEE Int Conf Robot Automat, pages 696–703, San Diego, CA, 1994.

Paredis CJJ, Khosla PK. Designing fault-tolerant manipulators: How many degrees of freedom? Int J Robot Res 1996; 15:611–628.

Roberts RG, Jamisola RS Jr, Maciejewski AA. Identifying the failure-tolerant workspace boundaries of a kinematically redundant manipulators. In IEEE Int Conf Robot Automat, pages 4517–4523, Roma, Italy, April 10-14, 2007.

Roberts RG, Maciejewski AA. A local measure of fault tolerance for kinematically redundant manipulators. IEEE Trans Robot Automat 1996; 12:543–552.

Roberts RG, Yu HG, Maciejewski AA. Characterizing optimally fault-tolerant manipulators based on relative manipulability indices. In IEEE/RSJ Int Conf Intell Robots Syst, pages 3925–3930, San Diego, CA, Oct 29-Nov 2, 2007.

Roberts RG, Yu HG, Maciejewski AA. Fundamental limitations on designing optimally fault-tolerant redundant manipulators. IEEE Trans Robot 2008; 24:1224–1237.

Srinivasa N, Grossberg S. A self-organizaing neural model for fault-tolerant control of redundant robots. In Int. Joint Conf Neural Networks, pages 483–488, Orlando, FL, Aug 12-17, 2007.

Sreevijayan D, Tosunoglu S, Tesar D. Architectures for fault-tolerant mechanical systems. In Medit Electrotech Conf, pages 1029–1033, Antalya, Turkey, Apr 12-14, 1994.

Tinos R, Terra MH, Bergerman M. Fault tolerance in cooperative manipulators. In IEEE Int Conf Robot Automat, pages 470–475, Washington, D.C., May 11-15, 2002.

Ukidve CS, McInroy JE, Jafari F. Using redundancy to optimize manipulability of stewart platforms. IEEE/ASME Trans Mechatron 2008; 13:475–479.

Yang JM. Fault-tolerant gaits of quadruped robot for locked joint failures. IEEE Trans Syst Man Cybern C 2002; 32:507–516.

Yi Y, McInroy JE, Chen Y. Fault tolerance of parallel manipulators using task space and kinematic redundancy. IEEE Trans Robot 2006; 22:1017–1021.